A Study of Aerodynamic Excitation Forces on a Radial Turbine Blade Due to Rotor-Stator Interaction

SATO Wataru : Manager, Turbo Machinery and Engine Technology Department, Products Development Center, Corporate Research & Development

YAMAGATA Akihiro : Manager, Turbo Machinery and Engine Technology Department, Products Development Center, Corporate Research & Development

HATTORI Hiroaki : Chief Engineer, Corporate Research & Development

It is important to predict the resonant vibration level for the design of a variable nozzle turbine. In this study, unsteady CFD analyses are conducted to investigate the flow mechanism that causes aerodynamic excitation forces. As a result, it was found that excitation forces are affected by shock waves and the nozzle clearance flow, and that these forces could be modeled by using one-dimensional aerodynamic parameters for the impeller inlet's dynamic pressure and Mach number. Furthermore, the resonant vibration level was calculated by conducting CFD and FEM analyses and then comparing the results with the experimental data. As a result, it has been confirmed that the CFD results can be used for qualitative evaluations of excitation forces.

1. Introduction

With growing awareness of the global warming issue, reducing automobile fuel consumption is being promoted as a way to reduce CO_2 emissions. One effective method of reducing fuel consumption is engine downsizing. Turbochargers are becoming widespread along with this concept as they make up for the low engine output of the smaller engines. A turbocharger is required to exhibit excellent responsiveness over a wide range of running conditions and especially during acceleration. In recent years, radial turbines that use a Variable Geometry System (VGS), that is, a mechanism that adjusts nozzle vane throats according to various engine operating conditions to control turbine output, have been used mainly for diesel engines. On the other hand, a VGS turbine requires that the aerodynamic excitation force be predicted during the design phase because the interaction between the nozzle vanes and the impeller causes periodic, unsteady pressure fluctuations to occur on impeller blade surfaces, and then these pressure fluctuations create an excitation force that causes blade vibration.

Recently, Computational Fluid Dynamics (CFD) has been utilized to conduct turbine unsteady flow analyses, and research has been actively conducted into quantitative assessments of vibration responses based on the prediction of aerodynamic excitation forces acting on impellers. Kawakubo[1] conducted unsteady CFD analysis using some different pressure ratios in combination with a fixed nozzle vane opening to assess the occurrence mechanism of aerodynamic excitation forces, clarifying that excitation forces acting on the leading edge of an impeller increased because of leakage flows created by nozzle vane clearances (hereinafter called nozzle clearance flows) and shock waves generated near nozzle vane trailing edges. Schwitzke, et al.[2] also conducted unsteady CFD analysis, demonstrating three flow mechanisms responsible for excitation forces, (i) rotor-stator potential interaction, (ii) nozzle vane wakes, and (iii) separated vortices near impeller blade leading edge on suction surfaces. However, although both the nozzle vane opening and the pressure ratio in a vehicle turbocharger vary depending on the specifications of and load on each engine, a systematic assessment of aerodynamic excitation forces acting on impellers was rarely conducted in previous research in terms of these two conditions.

This study therefore conducted unsteady CFD analysis using various conditions that differed in nozzle vane opening and pressure ratio and taking into account the rotor (impeller)-stator (nozzle vane) interaction, investigated the effects of different levels of nozzle vane opening and different pressure ratios on excitation force, and analyzed their mechanisms. In addition, the study identified aerodynamic parameters predominant over excitation forces from analysis results and demonstrated that excitation forces could be modeled in a simplified manner using those aerodynamic parameters. Finally, the study calculated vibration responses using CFD analysis and the Finite Element Method (FEM) and then compared test results, thereby verifying that the CFD analysis allowed qualitative assessments of excitation force.

2. Methodology

2.1 Subject of study

Figure 1 illustrates a CFD model of a turbocharger equipped with a VGS turbine. **Figure 1-(a)** shows a cutaway view. The turbine consists of multiple stationary parts, that is, the scroll and nozzle (VGS type), and one rotating part, that is, the impeller. **Figure 1-(b)** shows a cross-sectional view of the shaft (nozzle vanes and impeller) used for this analysis. The number of nozzle vanes was 14 and the number of impeller
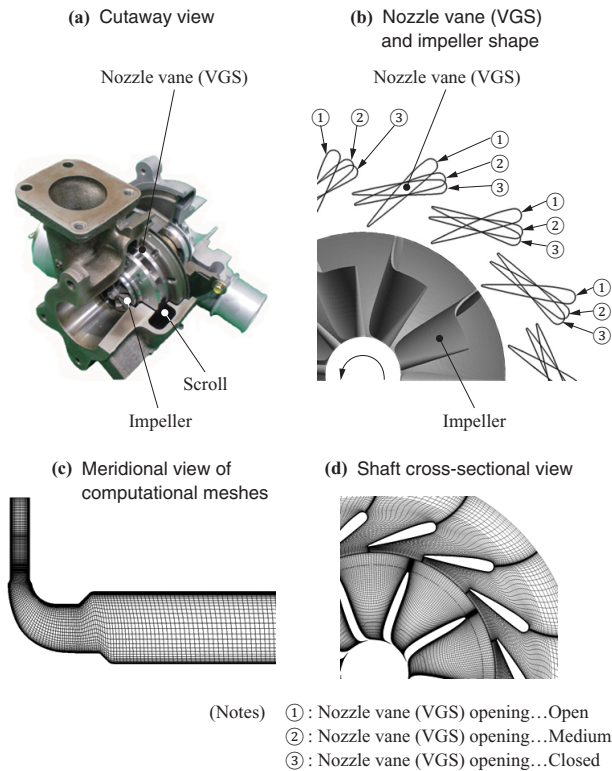
(a) Cutaway view

Nozzle vane (VGS)

Scroll

Impeller

(b) Nozzle vane (VGS) and impeller shape

Nozzle vane (VGS)

① ② ③

①
②
③

①
②
③

①
②
③

Impeller

(c) Meridional view of computational meshes

(d) Shaft cross-sectional view

(Notes)　① : Nozzle vane (VGS) opening…Open
　　　　② : Nozzle vane (VGS) opening…Medium
　　　　③ : Nozzle vane (VGS) opening…Closed

Fig. 1　CFD model

blades was 9. The impeller was approximately 50 mm in outside diameter. A VGS turbine is provided with clearances at the nozzle vane tips to ensure smooth operation of the nozzle vanes. This analysis also allowed for uniform clearances on both the hub and shroud sides, resulting in the clearances at the nozzle vane being 1.5% the span length of the nozzle vanes. We set three levels of nozzle vane opening: closed, medium, and open. By switching among the pressure ratio at each level of opening, we conducted analysis and took measurements of vibration responses.

2.2　Computation procedure

We used proprietary three-dimensional compressible unsteady CFD code. The code uses the MUSCL-Roe TVD scheme as the finite difference method for convective terms and uses the low Reynolds number Spalart-Allmaras model for eddy viscosity assessments. **Figure 1-(c)** shows a meridional view of the computational meshes, and **Fig. 1-(d)** shows a cross-sectional view of the shaft. An H-type structural grid is used for each blade passage. The computational domain only

covered the cascade ranging from the nozzle inlet to the impeller outlet, not including the scroll. This is because a VGS turbine is to suppress flow distortion within each nozzle passage caused by the scroll's non-axisymmetric geometry so that the effect on the impeller is reduced[3]. Meshes were created so that "y^+ < approximately 3" holds regarding the minimum size of the wall adjacent meshes, where y^+ = dimensionless wall distance. Since the number of nozzle vanes and the number of impeller blades were prime to each other, the unsteady CFD analysis required a full annulus model. Thus, the total number of meshes was no less than 16 million. Parallel computing was performed using a PC cluster in order to reduce computation time.

　The total pressure, total temperature, and swirl angle at the nozzle inlet were given as inlet boundary conditions, and the total pressure and swirl angle were predicted using a one-dimensional performance prediction model for the scroll. The impeller's speed of rotation was set to match the resonant frequency, as calculated from the impeller's eigen frequency and the number of nozzle vanes. **Table 1** shows computation cases investigated in this study and their respective conditions. Pressure ratio switching was performed by switching one inlet pressure to another with the outlet pressure kept constant.

　Figure 2 shows the procedure for calculating the aerodynamic excitation forces occurring on impeller blade surfaces from the unsteady CFD analysis results. The impeller interacts with flows from nozzle vanes, as shown in **Fig. 2-(a)**, resulting in the pressure difference between the pressure and suction surfaces becoming unsteady and causing the impeller blades to be subjected to excitation forces, as shown in **Fig. 2-(b)**. This unsteady pressure difference was analyzed using Fourier transform as shown in **Fig. 2-(c)**, and the pressure difference amplitude representing the first Vane

Table 1　Computational conditions

Item	Nozzle vane opening	Pressure ratio
Case 1	Closed	Low
Case 2	Closed	Medium
Case 3	Closed	High
Case 4	Medium	Low
Case 5	Medium	Medium
Case 6	Medium	High
Case 7	Open	Low
Case 8	Open	Medium

(a) Interaction between nozzle vanes and the impeller

Nozzle vane

Impeller

Direction of rotation

(b) Unsteady load on impeller blades

Normalized differential pressure (−)

1.0

0.0

−1.0

0　1　2　3
Normalized time　(−)

FFT

(c) FFT analysis

Normalized differential pressure amplitude (−)

1.0

0.5

0.0

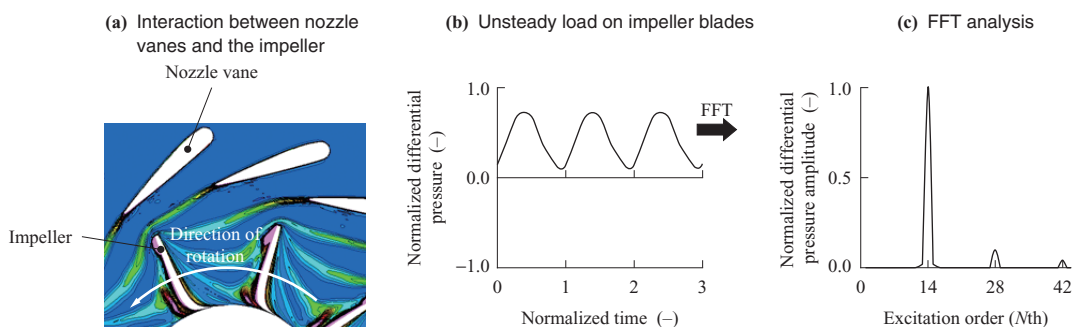0　14　28　42
Excitation order (Nth)

Fig. 2　Procedure for deriving excitation force

Passing Frequency (VPF) component was extracted and used to assess the magnitude of the excitation forces.

2.3 Experimental procedure

Figure 3 provides an overview of the non-intrusive vibration measurement system. Using optical sensors, this system irradiates the blade tips with a light beam and detects the reflected beam to record blade passing time. The system then calculates the difference between the blade passing time and the blade passing time measured without blade deformation, thereby determining the vibration response.

3. Results and discussion

3.1 Turbine performance

Figure 4 shows turbine performance characteristics derived from the unsteady CFD calculations. The pressure ratio, efficiency, and flow rate in the graphs are normalized by a ratio or difference relative to the representative value as follows: pressure ratio, the ratio to the medium pressure ratio; efficiency, the difference from the maximum efficiency; flow rate, the ratio to the maximum flow rate. When the nozzle vane open condition and the high pressure ratio were combined with each other, calculation was unstable and no results could be obtained.

3.2 Pressure ratio effect

Figure 5 shows the amplitudes representing the first VPF components of aerodynamic excitation force occurring on the impeller blades as derived from the unsteady CFD calculations. Whereas the amplitude of the aerodynamic excitation force increased with an increase in the pressure ratio at any level of nozzle vane opening (hereinafter called opening), the distribution of the force did not vary so widely. In order to quantitatively assess variations in pressure ratio effect among the three levels of opening, variations in excitation force — as expressed in terms of area-averaged amplitude of aerodynamic excitation force in the area adjacent to the impeller leading edge (from the leading edge to a point at a distance 0 to 10% of the blade length) — with respect to different levels of opening and different pressure ratios are shown in **Figs. 5-(b)** and **-(c)**. **Figure 5-(b)** shows that excitation force increased with an increase in the pressure ratio at every level of opening, showing also that the gradient varied depending on the level of opening. **Figure 5-(c)** shows $\Delta P/(0.5\rho_0 U^2)$, i.e., the normalized excitation force normalized by dynamic pressure calculated from ρ_0 (total density at the impeller inlet) and U (impeller's peripheral speed). At the open condition, the normalized excitation force remained unchanged even though the pressure ratio
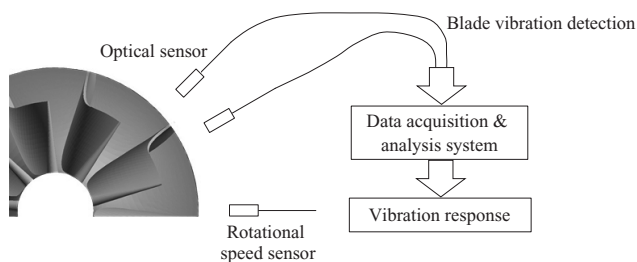

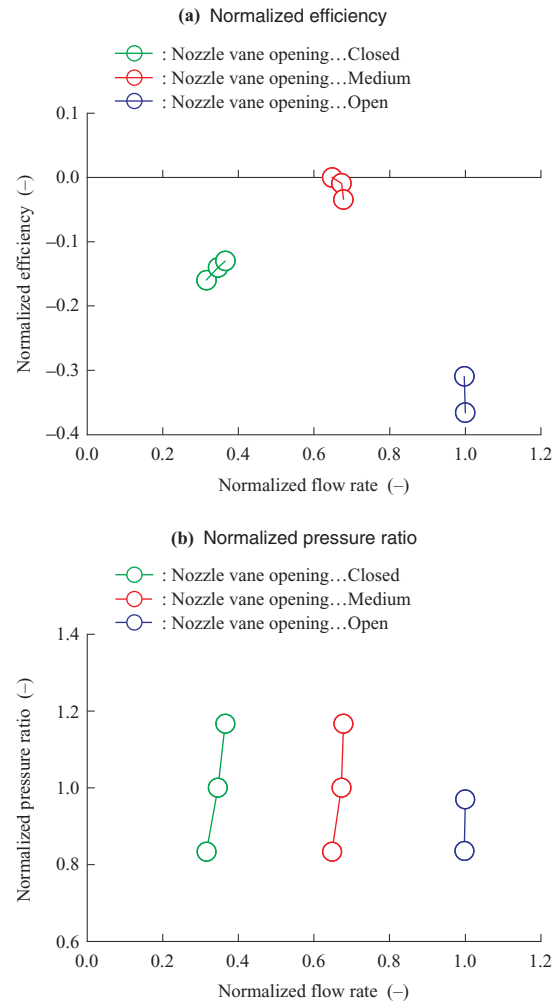Fig. 3 Non-intrusive stress measurement system

(a) Normalized efficiency

(b) Normalized pressure ratio

Fig. 4 Turbine performance characteristics predicted by using unsteady CFD

was changed, suggesting that excitation force varies in proportion to density. On the other hand, at the closed and medium opening, the normalized excitation force increased with an increase in pressure ratio. These effects of the pressure ratio are discussed below.

First, the results at the open condition are discussed. **Figure 6** shows the instantaneous Mach number and dilatation distributions at mid-span. At the open condition (**Fig. 6-(a)**), the flow was choked near the impeller trailing edge, and therefore the Mach number distribution between the nozzle and impeller remained unchanged although the pressure ratio was varied. Hence, the normalized excitation force also remained unchanged.

3.2.1 Shock wave effect

Next, the results at the closed and medium opening are discussed. As shown in **Fig. 6-(b)**, there was a region with a Mach number greater than 1 at the downstream side of the nozzle, unlike the case of "nozzle vane opening = open," and this region enlarged with an increase in the pressure ratio. Shock waves occurred near this region, and the dilatation distributions are shown in **Fig. 6-(c)** to assess the shock waves' strength. Dilatation was calculated using the divergence of velocity vectors, taking a value of 0 for an incompressible
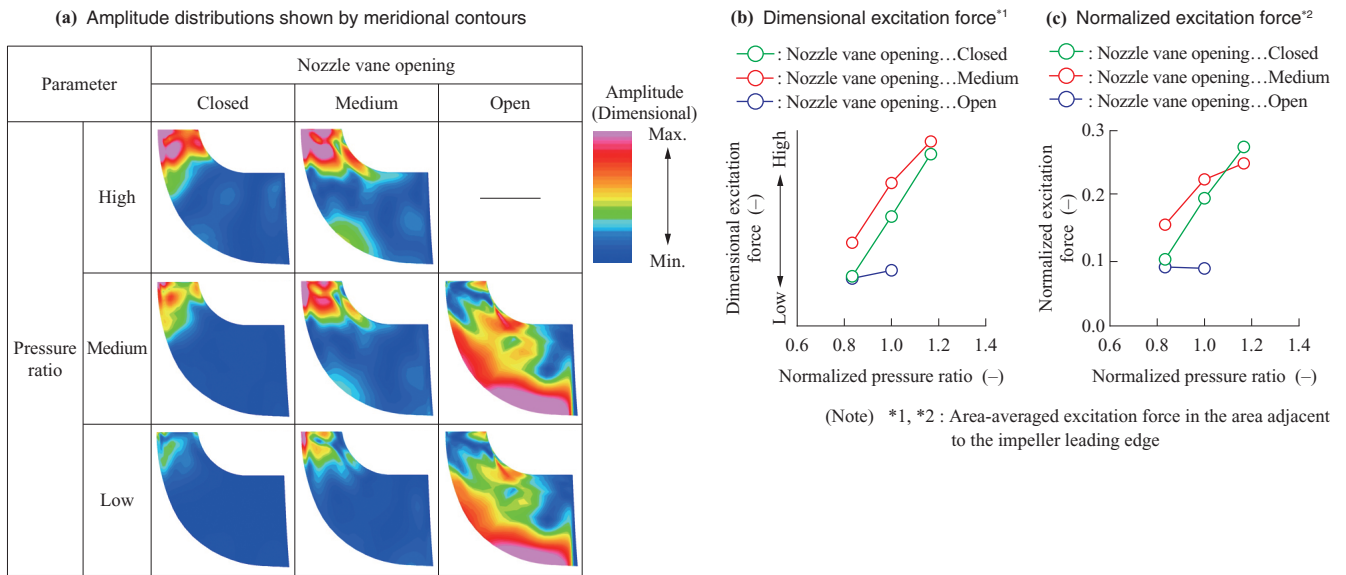
(a) Amplitude distributions shown by meridional contours

(b) Dimensional excitation force[*1]

(c) Normalized excitation force[*2]

(Note) *1, *2 : Area-averaged excitation force in the area adjacent to the impeller leading edge

Fig. 5   1st VPF component of excitation force exerted on impeller blade

(a) Mach number (Nozzle vane opening: Open)

(b) Mach number (Nozzle vane opening: Closed, Medium)

(c) Dilatation[*1]

(Note)   *1 : Divergence of velocity vectors
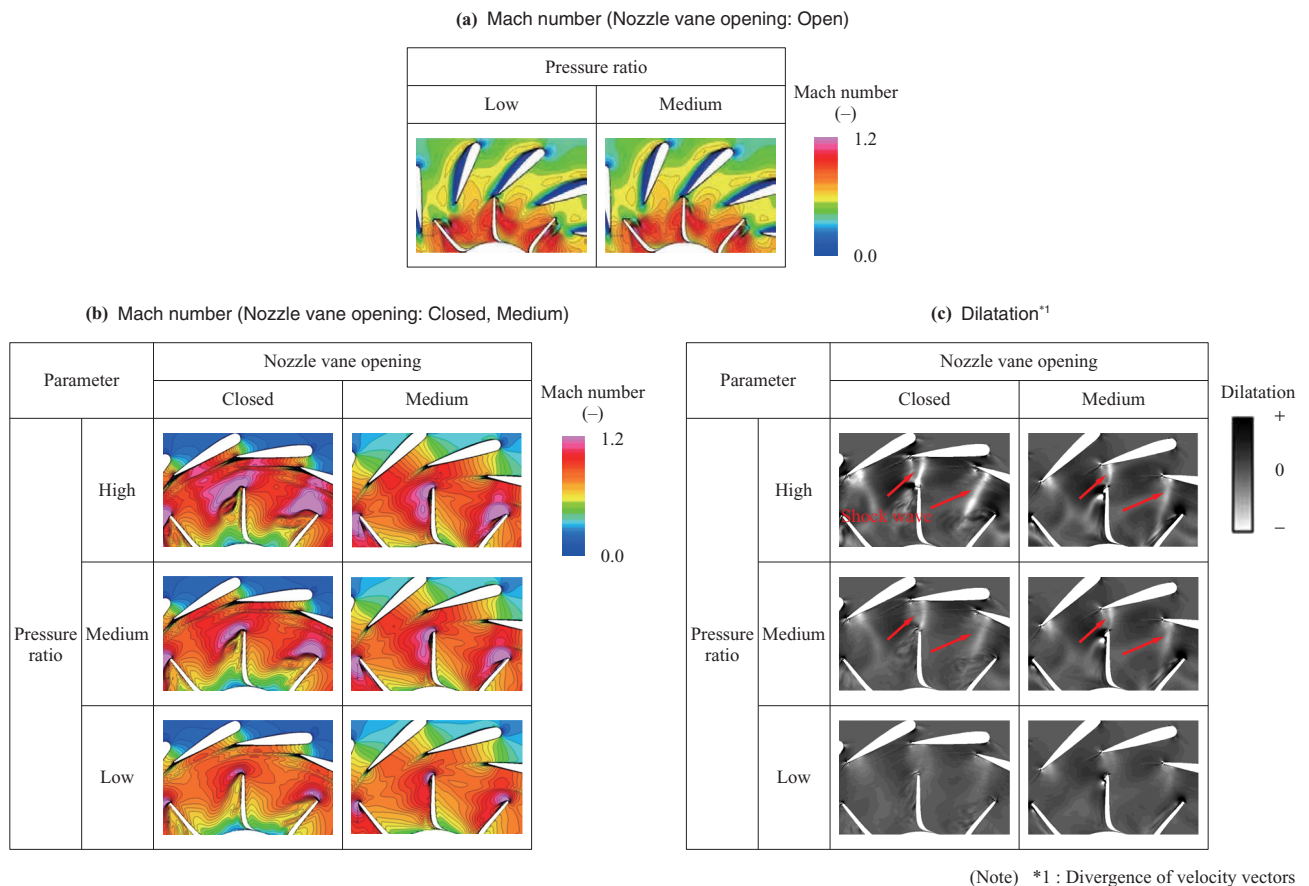
Fig. 6   Instantaneous Mach number and dilatation distribution at mid-span

flow field, a positive value for an expanding flow field, and a negative value for a contracting flow field. At the low pressure ratio, no shock waves were observed, but at the medium pressure ratio, weak shock waves were observed near the nozzle trailing edge. The shock waves grew in strength with an increase in the pressure ratio. It is thought that the impeller passed a strong pressure field created by the shock waves at the downstream side of the nozzle while the pressure field was subjected to disturbance, resulting in pressure fluctuations occurring on the impeller blades so as to strengthen the aerodynamic excitation force. Thus, at the closed and medium opening, not only density, but also shock

waves attributable to a high Mach number had a strong impact on the excitation force. In addition, the sensitivity of pressure ratios to the strength of shock waves at the closed opening was higher than that at the medium opening.

3.2.2 Effect of nozzle clearance flows

Figure 7 shows normalized excitation forces near the leading edge of the impeller and the effect of nozzle clearance flows. In order to assess the effect of nozzle clearance flows, normalized excitation forces near the impeller leading edge at the closed opening are shown in **Fig. 7-(a)** and those at the medium opening are shown in **Fig. 7-(b)**. **Figure 7-(c)** shows instantaneous velocity vectors near the hub end wall (absolute velocity vectors = blue for stationary parts, relative velocity vectors = red for rotating parts). Due to its radially inward absolute direction, a nozzle clearance flow affects the flow in a particular region in the impeller, resulting in the flow impinging on suction surfaces of the impeller blades (the impeller in **Fig. 7-(c)**, marked ① was in this situation) so as to cause a pressure rise. In a region not affected by the nozzle clearance flow, the flow is adequately diverted by nozzle vanes, so the flow did not impinge on suction surfaces. These two flow fields alternated with each other, resulting in an excitation force occurring on the hub side near the impeller leading edge and the shroud side. In addition, with an increase in the pressure ratio and load on the vanes, the impinge effect became larger. Thus, as shown in **Figs. 7-(a)** and **-(b)**, the pressure ratio increased not only in

the mid-span, which was significantly affected by shock waves, but also on the hub and shroud sides, which were affected by nozzle clearance flows, resulting in the normalized excitation force increasing. Moreover, the effect of pressure ratio variation was found to be more remarkable at the closed opening.

3.3 Correlations between the Mach number and normalized excitation force

This section extracts one-dimensional aerodynamic parameters that would be responsible for excitation force and discusses their correlations with excitation force in order to contribute to deriving a model formula to predict excitation force in a simplified manner in the early phase of turbine design. As described in **Sections 3.1** and **3.2**, excitation force was affected not only by density, but also by shock waves and nozzle clearance flows.

When there is high acceleration in the nozzle, that is, when the nozzle vane load and Mach number at nozzle outlet was high, the effects of shock waves and nozzle clearance flows were significant. **Figure 8** shows the correlations between the Mach number and normalized excitation force. Correlations at the open condition considerably differed from those at the closed and medium condition. Whereas the impeller incidence angle at the open condition was negative, the angle at the closed and medium condition was positive. Flow fields in the impeller at the open condition therefore greatly differed from those at the other levels of opening.
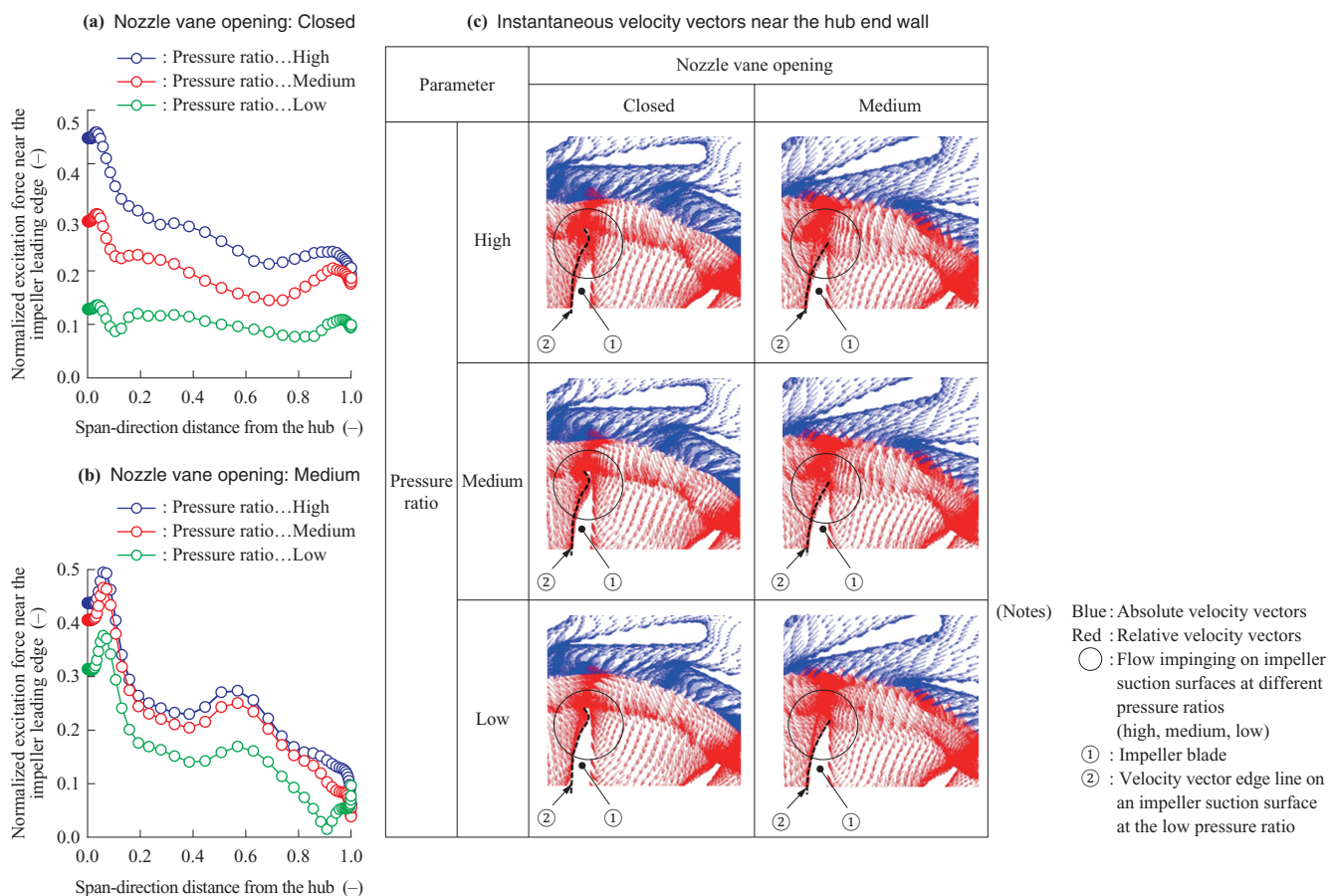

Fig. 7 Normalized excitation force near impeller L/E and effect of nozzle clearance flow
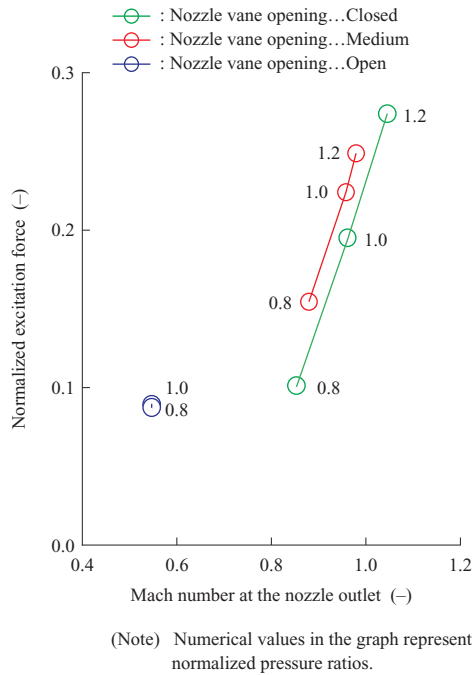
Fig. 8 Correlation between Mach number and normalized excitation force

(Note) Numerical values in the graph represent normalized pressure ratios.

This difference seems to be the reason for the aforementioned difference in correlations. At the closed and medium condition, the Mach number and normalized excitation force increased with an increase in the pressure ratio. Compared with the pressure ratio-normalized excitation force correlations, as shown in **Figs. 5-(b)** and **-(c)**, the Mach number had stronger correlations (stronger linearity) with the normalized excitation force, as shown in **Fig. 8**. In addition, correlations at the closed condition were virtually the same as those at the medium condition, and the correlations at both levels of opening could be approximated by a linear function. These characteristics are considered to be attributable to the relatively similar trends in the flow fields at the closed and medium condition, which were attributable in turn to the fact that the incidence angles at both levels of opening were close to each other.

The aforementioned results suggest that excitation force can be modeled using one-dimensional aerodynamic parameters (dynamic pressure and Mach number at the impeller inlet), suggesting also that in addition to three-dimensional unsteady CFD analysis, one-dimensional steady flow calculation makes it possible to predict excitation force in a simplified manner in the early phase of turbine design. Our next task is to verify correlations between excitation force and aerodynamic parameters for other types of turbines and derive a generally applicable model formula.

3.4 Comparison between predicted and measured vibration responses

Finally, we compared the vibration response prediction results with the test results to validate our CFD analysis. Prediction was performed using both unsteady CFD analysis and FEM. ANSYS was used as the FEM solver. **Figure 9** shows vibration response prediction results and test results

normalized by the respective maximum values. The prediction matched the measurement well with respect to the sensitivity of the pressure ratios to vibration responses at the closed condition. At the medium opening, however, the sensitivity of the prediction was about half the measurement. On the other hand, both the prediction and measurement showed a trend in which the sensitivity of the pressure ratios declined with an increase in opening. Based on these comparison results, it can be said that our CFD analysis
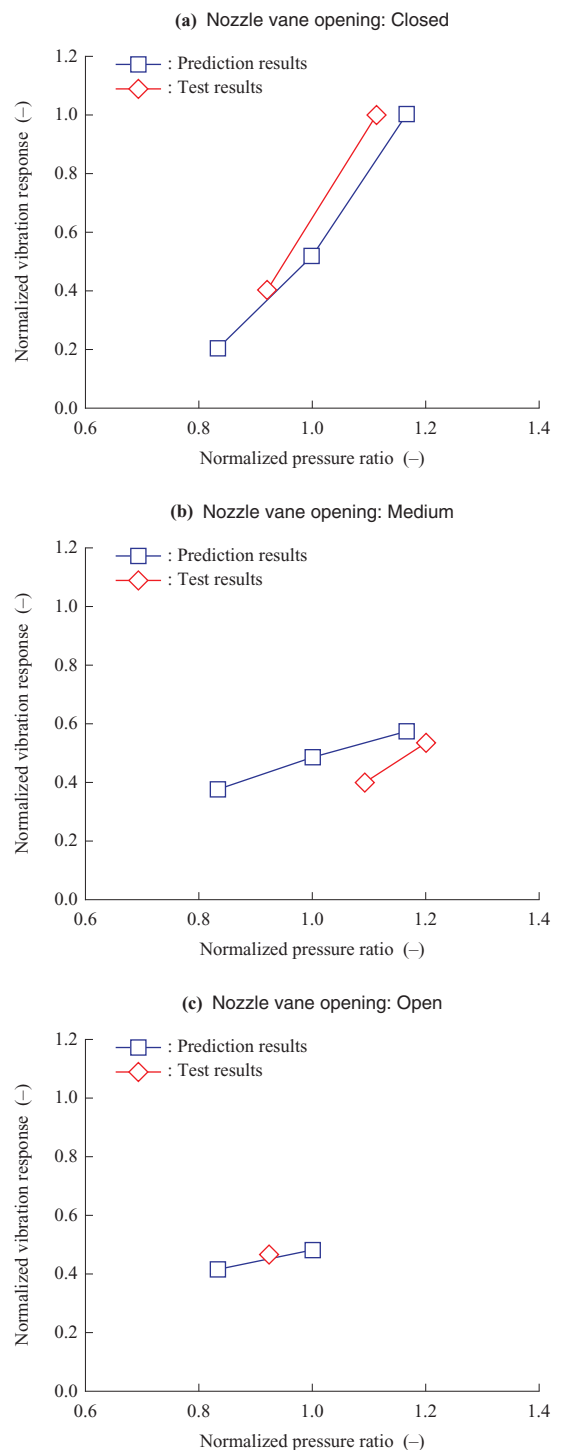

Fig. 9 Comparison of predicted and measured resonant vibration levels

could qualitatively grasp the effects of different levels of opening and different pressure ratios on excitation force while the analysis did show quantitative deviations with regard to some of the parameters.

4. Conclusion

In order to investigate the effects of different levels of nozzle vane opening and different pressure ratios on impeller excitation force, we conducted unsteady CFD analysis on a VGS turbine. In addition, we compared vibration response prediction results with test results, thereby validating the CFD analysis. As a result, we have derived the following conclusions:

(1) At the nozzle vane open condition, choked flows occurred near the impeller trailing edge. Therefore, Mach number distribution remained unchanged even though the pressure ratio was changed, and excitation force varied in proportion to the density at the impeller inlet.

(2) At the nozzle vane closed and medium condition, the effects of shock waves and nozzle clearance flows on excitation force were intensified when the pressure ratio and the Mach number were higher. In addition, this phenomenon was more remarkable at the closed condition.

(3) Excitation force can be modeled using one-dimensional aerodynamic parameters (dynamic pressure and Mach number at the impeller inlet) in order to predict excitation force in a simplified manner in the early phase of turbine design.

(4) Our CFD analysis qualitatively grasped the effects of different levels of nozzle vane opening and different pressure ratios on excitation force.

REFERENCES

(1) T. Kawakubo : Unsteady Rotor-Stator Interaction of a Radial-Inflow Turbine With Variable Nozzle Vanes ASME Proceedings Turbomachinery Paper No. GT2010-23677 (2010. 6) pp. 1-10

(2) M. Schwitzke, A. Schulz and H. -J. Bauer : Numerical analysis of aerodynamic excitation of blade vibrations due to nozzle guide vanes in radial inflow turbines ISROMAC-14 (2012)

(3) S. Ota and T. Kawakubo : A Numerical Study on the Three-Dimensional Flows in the Scrolls and Nozzles of a Radial Turbine for a Variable Geometry Automotive Turbocharger International Gas Turbine Congress 2007 Tokyo TS-028 (2007. 12)

(4) W. Sato, A. Yamagata and H. Hattori : A study on unsteady aerodynamic excitation forces on radial turbine blade due to rotor-stator interaction 11th International Conference on Turbochargers and Turbocharging (2014. 5) pp. 389-398